Effect of Different Doses of Silver Nanoparticles on Lung and Cardiac Muscle of Adult Female Albino Rat (A Histological and Immunohistochemical Study)

Original Article

Suzan Elsayed Abo Elnasr [1], Ayah Mohamed Hassan Ragab[2], Mohamed Hassan Ragab[3] and Shaimaa Mohammed Zaher[4]

[1]Department of Histology and Cell Biology, [3]Department of Anatomy, Faculty of Medicine, Tanta University, Egypt.

[2]Department of Reproductive Health and Family Planning, National Research Centre, Giza, Egypt.

[4]Department of Histology and Cell Biology, Faculty of Medicine, Helwan University, Egypt.

ABSTRACT

Introduction: Many potential applications of silver nanoparticles (Ag NPs), which include diagnostics, antimicrobial agents, and cancer therapy, have made them a popular subject of study in recent years. Despite their importance and widespread use, they may cause environmental and human toxicity.

Aim of the Work: To assess outcomes of different Ag NPs doses on adult female albino rat's lung and cardiac muscle histologically and immunohistochemically.

Materials and Methods: 30 adult female albino rats were randomly divided into 3 groups: control (group I), group II received 30 mg/kg Ag NPs, and group III received 300 mg/kg. Groups II and III received Ag NPs orally daily for two weeks. Lung and cardiac muscle specimens were histologically and immunohistochemically processed. Studies employing morphometry and statistics were conducted as well.

Results: Lung specimens from Ag NPs treated animals showed collapse of some alveoli, emphysematous dilatation to others and thickening of the interalveolar septa. Collagen fibers were deposited. Congested blood vessels, hemorrhage areas, and inflammatory cells were seen. Immunohistochemical results showed an increase in the cytoplasmic reaction for CD-68. Cardiac muscle specimens showed extravasated RBCs and congested blood vessels. Inflammatory cellular infiltration and vacuolation of cardiac muscle fibers were noticed. Cardiac muscle fibers exhibited interruption with wide spaces and deposition of collagen fibers between them. Cleaved caspase 3 optical density in cardiomyocytes increased significantly. Group III experienced all these changes to a greater degree than group II.

Conclusion: The findings of the present study indicate that subjection to Ag NPs may cause cardiac and pulmonary histological and immunohistochemical alterations which may affect the function of these vital organs.

Received: 26 June 2023, **Accepted:** 05 July 2023

Key Words: Cardiac muscle, CD68, cleaved caspase3, lung, silver nanoparticles.

Corresponding Author: Suzan Elsayed Abo Elnasr, MD, Department of Histology and Cell Biology, Faculty of Medicine, Tanta University, Tanta, Egypt. **Tel.** +2 010 0074 8926, **E-mail:** souzan.emamo@med.tanta.edu.eg

ISSN: 1110-0559, Vol. 47, No. 3

INTRODUCTION

One of today's most significant and promising scientific fields is nanotechnology. This technology deals with small sized compounds, called nanoparticles (NPs) which are natural or manufactured materials with diameter ranging from 1 to 100 nm[1,2]. NPs are classified into organic, and inorganic based on physical and chemical characteristics. Organic nanoparticles incorporate carbon NPs whereas, inorganic nanoparticles include semi-conductor (as zinc oxide) ,magnetic (like cobalt and iron), metal-based (as gold and silver) and lipid-based NPs (as liposomes, solid lipid nanoparticles)[3,4].

Ag NPs are among the most widely applied nanometals. Silver is widely used due to its conductivity, chemical stability, catalytic activity, and high surface area to volume ratio[5,6].

The antimicrobial activity of Ag NPs is effective against more than 650 various organisms, including bacteria, viruses, and fungi. Ag NPs' antimicrobial properties make them useful in the medical field, food preservation, textile coating, optical sensors, and orthopedics[5,7]. Additionally, branded products as sunscreen, medical masks, cosmetics, bone cement, toothpaste, dental resin composite, deodorants, and shampoo are coated with Ag

DOI: 10.21608/ejh.2023.202533.1875

NPs. Moreover, many other products are also coated with Ag NPs including washing machines, refrigerators, and air conditioners. Ag NPs are also used in many available products as medical shoes, sport shirts, toys, baby pacifiers[8,9]. Numerous reports showed that Ag NPs can be targeted to specifically kill cancer cells and may be toxic to them[10,11]. Nanobiomedicine uses Ag NPs in vaccine nanovectors, drug-delivery systems, and diagnostic platforms[12].

Despite the importance and widespread use of Ag NPs, they may cause environmental and human toxicity. During manufacturing, Ag NPs may release into the environment. This occurs via several processes, as particle synthesis during manufacturing and incorporation into products, recycling, and disposal[13]. According to nano studies, Ag NPs' toxicity may be related to the charge and functional groups on their surface as well as their capacity to bind to or interact with cellular components, producing hydrogen peroxide and reactive oxidative species (ROS) that may harm the plasmalemma and cytoplasmic organelles, particularly the mitochondria as well as cytoskeleton[9].

De matteis,[14] reported that there were several methods for Ag NPs entry. These included inhalation, dermal contact, intraperitoneal in addition to intravenous injection. Ingested silver can move to different organs in the body, leading to various health risks[15,16].

Ag NPs are inhaled during the production of materials containing silver as well as when using aerosolized goods, allowing these particles to enter lung tissue. The distribution of inhaled Ag NPs to extra-pulmonary organs like the liver, brain, kidney, heart, and intestine is also possible[17].

Previous studies demonstrated histopathological alterations caused by different sizes of Ag NPs on vital organs as kidney, liver, and testes[8,9&18]. Thus, this study examined how different Ag NPs' doses affected the lung and cardiac muscle histology of adult female albino rats.

MATERIALS AND METHODS

Reagents

Ag NPs preparation

Ag NPs (puress, Fluka) in the amount of $5x10^{-3}$ mol dm^{-3} were produced by citrate reduction using the Turkevich protocol. One hundred ml of double-distilled H_2O were combined with 0.0850 gram of silver nitrate. Next, 25 ml of the stock solution was added to one hundred ml of double-distilled H_2O. The solution was warmed till boiled. With vigorous magnetic swirling, 5 ml of a 1% sodium citrate was added to the boiling solution, and heating was continued until the solution became yellow. Double-distilled H_2O was used to dilute Ag NPs solution to 125 ml, and it was kept at 4 °C[19]. The aqueous Ag NPs dispersion was dropped onto a carbon-coated copper grid and dried with air at room temperature before microscope examination. Transmission electron microscopy (TEM, Hitachi HU-11B) at an 80 kV voltage was employed to investigate the particles size as well as the shape of the Ag NPs. The nanoparticles diameter was 20 nm.

Using a cell made of quartz with a pathlength of 1 cm, the electronic UV-Visible spectra of absorption were collected using a Perkin Elmer lambda-17 spectrophotometer. The prepared particles showed absorption in the visible range due to Surface Plasmon Resonance at 405 nm and the TEM showed that the particles were spherical with very good size distribution. At the National Research Center in Giza, Egypt, this procedure was carried out.

Animals

This study used 30 adult female Wister albino rats, varying in age from 12 to 14 weeks and weighing in range of (140-160 grams). Before and during the experiment, they were housed in cages that met all safety requirements and had plenty of ventilation. For two weeks, they were exposed to the normal conditions of an animal cage. The Faculty of Medicine at Tanta University in Egypt's ethical committee gave its approval to the current work (Approval number: 35906).

Study design

Three groups of ten rats were formed:

Group I: (control) was divided into 2 equal subgroups:

- Subgroup (i): 5 rats untreated throughout the experiment.
- Subgroup (ii): 5 rats, each received 1.5 ml of double distilled H_2O (the vehicle for nanoparticles) via oral route every day for two weeks.

Group II: included 10 rats, each received low dose of Ag NPs (30 mg/kg) (suspended in 1.5 ml double distilled H_2O) via oral route every day for two weeks[20,21].

Group III: included 10 rats, each received high dose of Ag NPs (300 mg/kg) (suspended in 1.5 ml double distilled H_2O) via oral route every day for two weeks.[20,21].

To render all animals unconscious at the end of the experiment, sodium pentobarbital (50 mg/kg) was administered intraperitoneally to each animal[22]. Lung and left ventricle heart tissue specimens were taken out and processed histologically and immunohistochemically.

Light microscopy preparation

The lung and left ventricle heart tissue were fixed in formalin and embedded in paraffin blocks for histological analysis. 5-micrometer serial histological sections were cut and examined using:

1. Hematoxylin and eosin stain to assess structure of lung and cardiac muscle tissues histologically[23].
2. Masson`s trichrome stain for collagen fibers demonstration[24].
3. Immunohistochemical staining using the avidin-biotin-peroxidase complex technique[25] for demonstration of:

A- CD-68 (In lung specimens, as an indicator of alveolar macrophage) using anti CD-68 antibody (mouse monoclonal antibody, Leica Biosystems, Benton La, Newcastle Ltd, UK; code NCL-L-CD68, 1:200 dilution).

B- Cleaved Caspase 3 (as a sign of apoptosis in samples of cardiac muscle) using anti cleaved caspase 3 antibody (polyclonal rabbit active/cleaved caspase 3 antibody, Cell Signaling Technology, Danvers, USA; cat no. 9661, dilution 1:100).

Paraffin sections, 5 microns thick, were dewaxed in xylene and rehydrated in ethanol (descending grades). Hydrogen peroxide inhibited endogenous peroxidase activity at 0.3 percent. After performing heat-induced antigen retrieval by microwaving with citrate buffer pH 6.0 (10 Mm, 20 min), at room temperature, tissue sections were incubated with primary antibody overnight. Streptavidin biotin complex detection method was used in the second step of staining. Finally, the sections were stained for 5-10 minutes with diaminobenzidine (DAB) solution (as chromogen), rinsed 3 times in phosphate buffered saline (PBS) for two minutes each, and counterstained with Mayer hematoxylin. Without primary antibody, negative control was done.

Positive control for CD-68 antibody was liver Kupffer`s cells (according to data sheet of manufacturer) and its positive immunoreactivity appeared as brown cytoplasmic staining in the macrophages[26]. The pancreas section was the positive control for cleaved caspase-3 antibody (according to data sheet of manufacturer) and its positive reaction was brown cytoplasmic or nuclear[27]. The prepared slides were examined and photographed by Olympus light microscope with an integrated camera in Histology and Cell Biology department of Faculty of Medicine, Tanta University.

Morphometric study

Image J version (1.48) measured 10 non-overlapping fields from each slide in each group, (National Institutes of Health, Bethesda, Maryland, USA), demonstrating:

1. Area percentage of collagen fibers in Masson`s trichrome stained sections (X200) in lung and cardiac muscle specimens[26, 28].
2. The optical density of CD-68 immunoreactivity (X400)[29] in lung sections.
3. The optical density of cleaved caspase 3 immunoreactivity (X400)[29] in cardiac muscle sections.

Statistical analysis

One-way ANOVA and Tukey's test were used to compare estimated numbers. The entire set of data was expressed using the mean and standard deviation. If probability value (*P-value*) was less than 0.05, differences were significant[30].

RESULTS

No deaths occurred during the duration of the experiment. The histological findings were identical in both subcategories of the control group. Thus, they served as a control group.

Results of lung specimens

IA- Light Microscopic Examination of the Lung

1-Hematoxylin and Eosin stained sections

Examination of group I lung sections revealed that they had the same known histological structure of the lung. The lung was formed of sac like structures (alveoli), alveolar sacs and alveolar ducts. Between the alveoli, there were thin interalveolar septa. Aside from the thin-walled blood vessels, the simple columnar ciliated epithelium of bronchioles and the thin smooth muscle layer surrounding their wall were also observed (Figure1). Simple squamous type I pneumocytes and simple cuboibal type II pneumocytes were seen to line alveolar wall with higher magnification (Figure 2).

Meanwhile, examination of group II showed variation in the changes which were focal in some sections and diffuse in others. Collapse of some alveoli was observed while emphysematous dilatation to others was noticed. The interalveolar septa were thickened. Congested blood vessels and areas of hemorrhage were observed within lung interstitium as well as desquamated epithelial cells in the bronchiolar lumen. Moreover, some inflammatory cells were noticed between alveoli (Figures 3,4,5).

Regarding group III, there was severe destruction to the architecture of the alveoli. In some sections, most of alveoli were full of red blood cells (Figure 6) while in other sections, alveoli became dilated and irregular in shape (Figure7). Collapse of some alveoli and emphysematous dilatation to others were also noticed (Figure 8). Moreover, the bronchioles showed vacuolation of their epithelial cells. Dilatation and congestion of blood vessels as well as inflammatory cellular infiltration were seen (Figures 7,8,9).

2-Masson's trichrome stained sections

Very few collagen fibers were detected around alveoli and blood vessels in control group (Figure10). Group II, on the other hand, showed an apparent moderate amount of collagen fibers around bronchioles and around dilated, congested blood vessels (Figure11). Additionally, group III revealed marked collagen fiber in the interstitium of lung and around dilated, congested blood vessels (Figure12).

3- CD-68 immunohistochemically stained sections

Control group showed weak positive CD-68 cytoplasmic immunoreaction in few alveolar macrophages in interalveolar septa (Figure13). Group II had more alveolar macrophages with moderate cytoplasmic immunoreaction (Figure14). Many alveolar macrophages of group III showed strong CD-68 cytoplasmic immunoreaction (Figure15).

IB-Morphometric results & statistical analysis

The mean area percentage of collagen fibers

increased significantly (p<0.05) in group II and highly significantly (p <0.001) in group III compared to the control group. Group III had more collagen fibers than group II, but the difference was not significant (p > 0.05) (Table 1, Histogram 1. A).

Group III had a highly significant rise in CD-68 mean optical density (p <0.001), while group II had a significant rise (p <0.05) in comparison to control group. In group III, mean CD-68 optical density elevated significantly (p < 0.05) in relation to group II (Table 1, Histogram 1.B).

II-Results of cardiac muscle specimens

IIA-Light Microscopic Examination of the Cardiac Muscle

1-Hematoxylin and Eosin stained section

Cardiac muscle sections from control group's left ventricles showed branched and anastomosed fibers. Cardiac myocytes exhibited acidophilic sarcoplasm with oval, central open face nuclei. Between cardiac muscle fibers there was a loose connective tissue containing blood vessels and fibroblasts with flat dark nuclei (Figure 16 A, B).

Group II, showed alterations in the cardiac muscle's histological structure as extravasation of RBCs and inflammatory cell infiltration in areas between fibers. Fibers of the cardiac muscle were disorganized and appeared wavy with areas of low acidophilia. The cardiac muscle fibers were widely separated and interruption of some of them was also seen (Figures 17,18). Regarding cardiac myocytes, pyknotic nuclei were noticed (Figure19).

Regarding group III, there was severe destruction of cardiac muscle. Extravasated RBCs and foci of muscle hyalinosis (homogenous acidophilic areas of the sarcoplasm) were observed (Figures. 20,21). Blood vessels were dilated and congested with inflammatory cellular infiltration and vacuolated cardiac muscle fibers. Cardiac muscle fibers exhibited fragmentation, hyper-acidophilic areas, interruption, and wide spaces between them (Figures 21, 22, 23 ,24). Pyknotic nuclei of some cardiac myocytes were also noticed (Figure. 25).

2-Masson's trichrome stained sections

Sections of cardiac muscle from left ventricles of the control group showed minimal amounts of collagen fibers in connective tissue spaces among the cardiac muscle fibers (Figure 26). Whereas group II demonstrated elevated collagen fiber deposition around dilated blood vessels and among fibers of cardiac muscle (Figure 27). Also, in group III collagen fiber deposition increased around dilated blood vessels and among cardiac muscle fibers (Figure 28 A,B).

3-Cleaved Caspase 3 immunohistochemically stained sections

Control group had negative cleaved caspase-3 reaction (Figure 29). While group II showed moderate positive reaction in some cardiomyocytes (Figure 30). Group III showed strong positive reaction in many cardiac myocytes (Figure31).

IIB-Morphometric results & statistical analysis

Group III had a significant rise in mean percentage area of collagen fibers (p < 0.05) relative to the control group. While there was a nonsignificant rise (p >0.05) in group II relative to control group and in group III relative to group II (Table 2, Histogram 2. C).

The mean optical density of cleaved caspase 3 in groups III and II showed a highly significant elevation (p < 0.001) relative to control group. There was nonsignificant rise in group III (p >0.05) relative to group II (Table 2, Histogram 2. D).

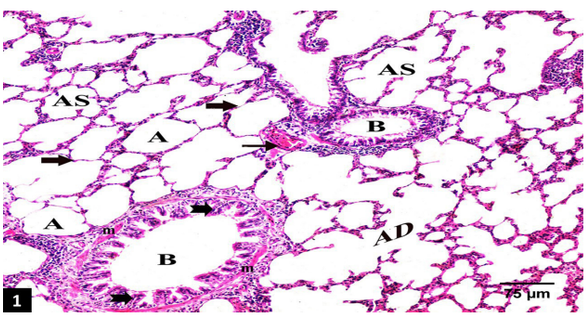

Fig.1: A photomicrograph of a lung section of control group showing normal lung architecture with normal alveoli (A), alveolar sacs (AS) and alveolar ducts (AD) with thin interalveolar septa (thick arrows). Normal bronchioles (B) with their simple columnar ciliated lining epithelium (notched arrows) and smooth muscle layer (m) surrounding their wall are also noticed. Note the thin walled blood vessels (thin arrow) (H and E ×200).

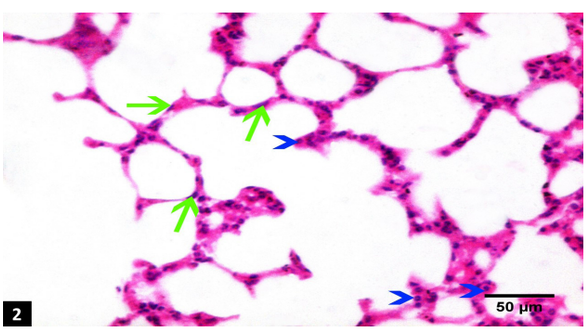

Fig.2: A photomicrograph of a lung section of control group showing lung alveoli lined with simple squamous type I pneumocytes (green arrows) and simple cuboidal type II pneumocytes (blue arrow heads). (H and E ×400).

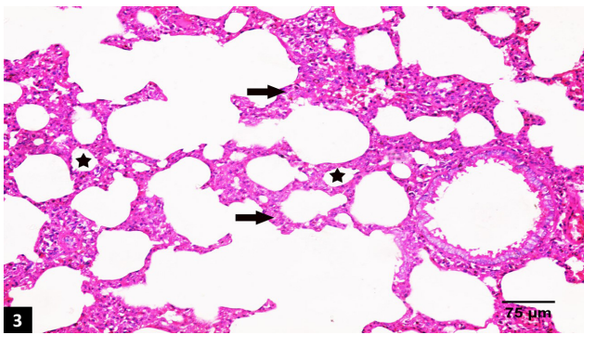

Fig.3: A photomicrograph of a section of lung of group II (animals received low dose of Ag NPs) showing collapse of some alveoli (stars) with thickening of the interalveolar septa (thick arrows). (H &E x 200)

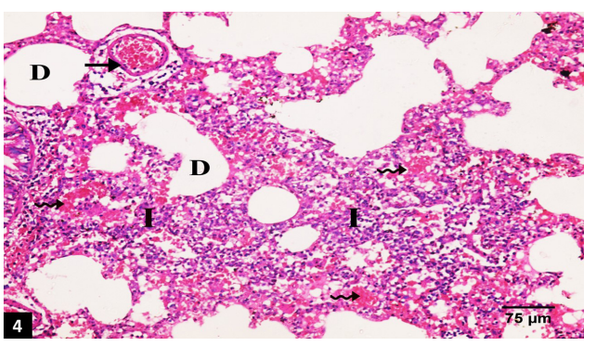

Fig.4: A photomicrograph of a section of lung of group II (animals received low dose of Ag NPs) showing emphysematous dilation (D) of some alveoli with areas of hemorrhage (zigzag arrows) and congested blood vessels (thin arrow). Infiltration of inflammatory cells (I) is also observed within lung interstitium. (H &E x 200)

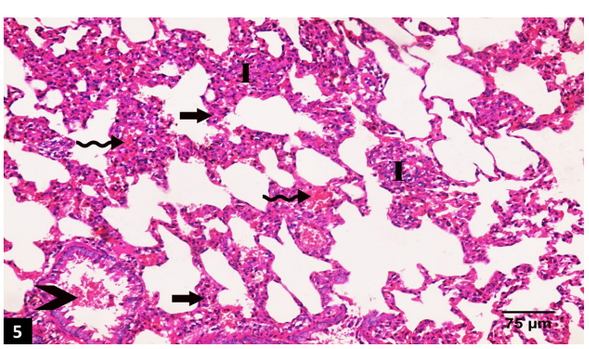

Fig.5: A photomicrograph of a section in the lung of group II (animals received low dose of Ag NPs) showing thickening of the interalveolar septum (thick arrows), hemorrhage (zigzag arrows) within lung interstitium and desquamated epithelial cells in bronchiolar lumen (arrow head). Some inflammatory cells (I) are observed between alveoli. (H &E x200)

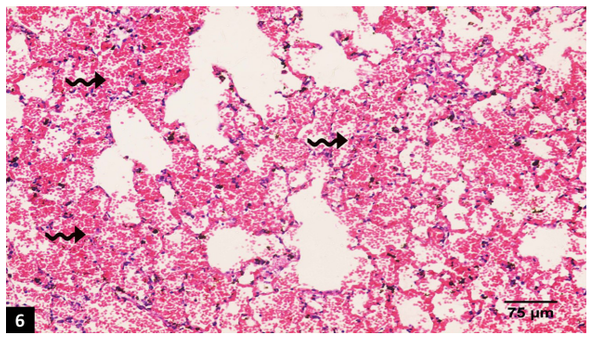

Fig.6: A photomicrograph of a section of lung of group III (animals received high dose of Ag NPs) showing disturbance in the architecture of the alveoli and most of them are full of red blood cells (zigzag arrows) (H &E x 200).

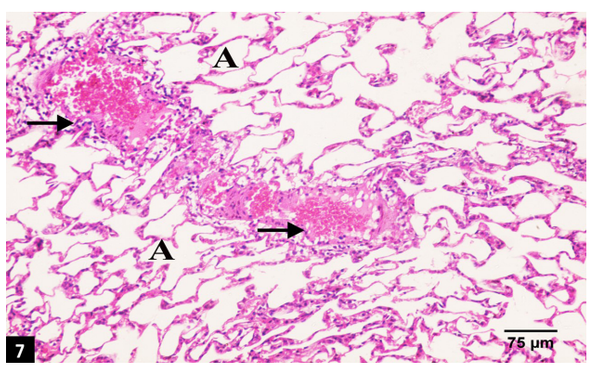

Fig.7: A photomicrograph of a section of lung of group III (animals received high dose of Ag NPs) showing disturbance in the architecture of the alveoli that become dilated and irregular in shape (A) and congested dilated blood vessels (thin arrows) in between them (H &E x200).

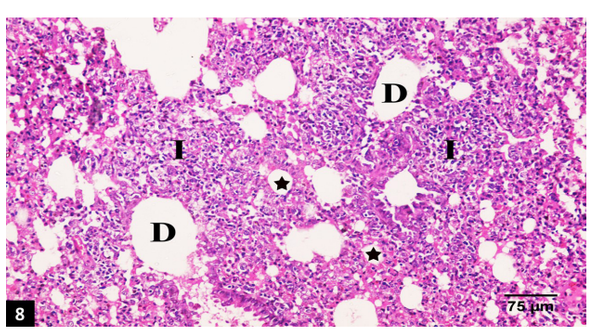

Fig.8: A photomicrograph of a section of lung of group III (animals received high dose of Ag NPs) showing some alveoli collapsed (stars) others with emphysematous dilatation (D). Inflammatory cellular infiltration (I) is also noticed within lung interstitium. (H &E x 200).

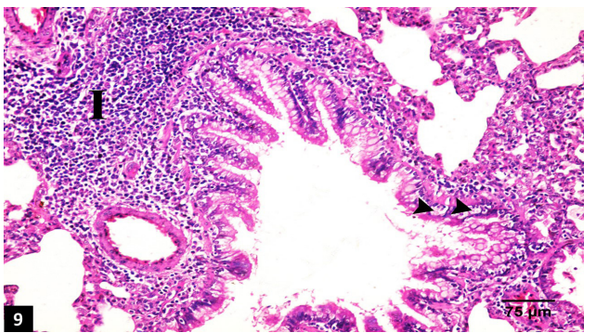

Fig.9: A photomicrograph of a section of lung of group III (animals received high dose of Ag NPs) showing vacuolation of the bronchiolar epithelial cells (arrow heads) and infiltration of inflammatory cells (I) in between the bronchioles and alveoli. (H &E x 200).

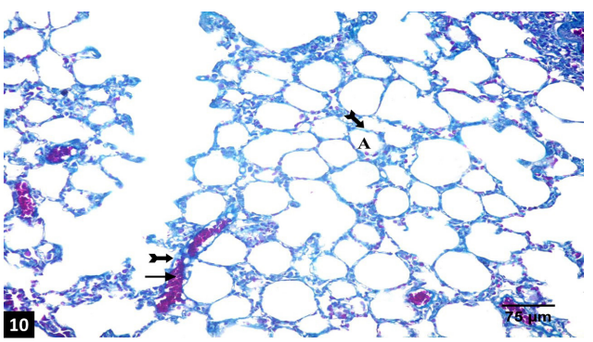

Fig.10: A photomicrograph of a section of lung of control group showing minimal collagen fibers (bifid arrows) deposition around alveoli (A) and blood vessels (thin arrow). (Masson`s trichrome x 200).

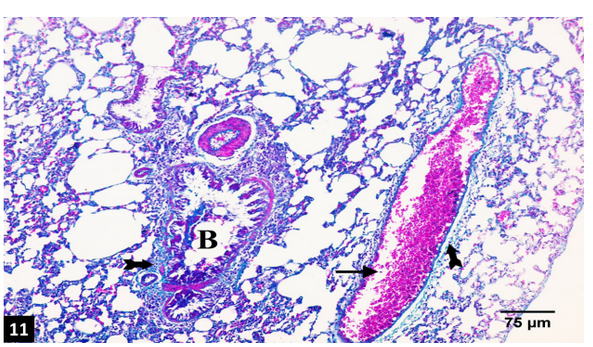

Fig.11: A photomicrograph of a section of lung of group II (animals received low dose of Ag NPs) showing apparent deposition of moderate amount of collagen fibers (bifid arrows) around bronchioles (B) and around the dilated congested blood vessels (thin arrow). (Masson`s trichrome x 200).

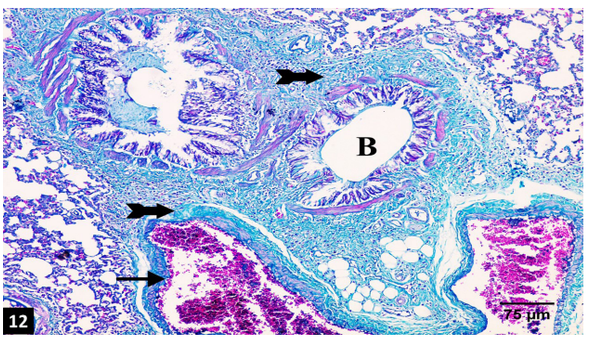

Fig.12: A photomicrograph of a section of lung of group III (animals received high dose of Ag NPs) showing marked collagen fibers deposition (bifid arrows) around bronchioles (B) and around the dilated congested blood vessels (thin arrow). (Masson`s trichrome x 200).

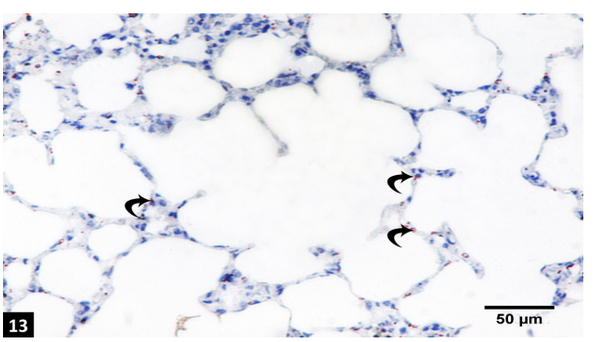

Fig.13: A photomicrograph of a section in the lung of control group showing mild positive cytoplasmic reaction for CD68 (curved arrows) in few alveolar macrophages in the interalveolar septa. (CD-68 Immunostaining x 400).

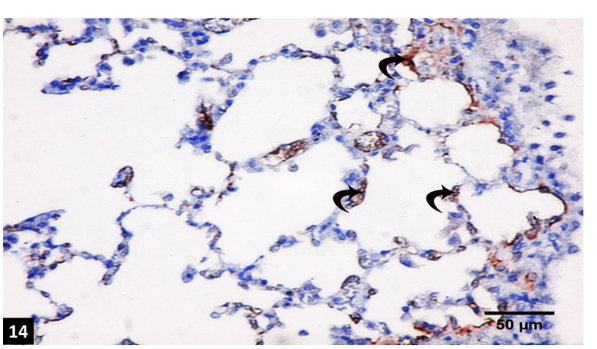

Fig.14: A photomicrograph of a section in the lung of group II (animals received low dose of Ag NPs) showing apparent increase in the positive reaction for CD 68 (curved arrows) in some macrophages of the interalveolar septum. (CD-68 Immunostaining x 400).

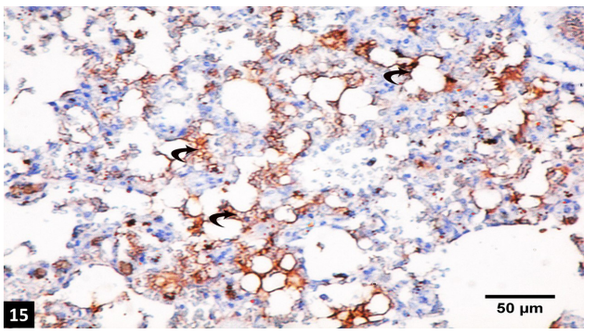

Fig.15: A photomicrograph of a section of lung of group III (animals received high dose of Ag NPs) showing apparent strong positive cytoplasmic immunoreaction for CD68 in many alveolar macrophages (curved arrows). (CD68 Immunostaining x 400).

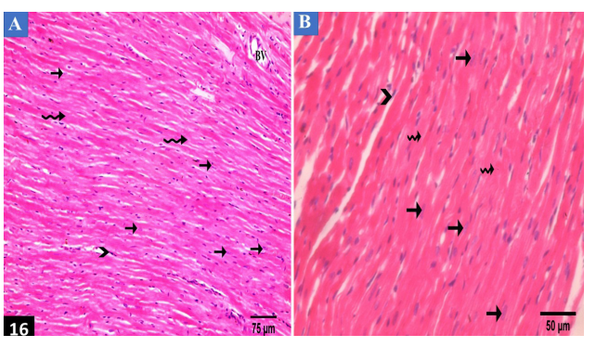

Fig.16: photomicrographs of longitudinal sections (LS) in the cardiac muscle of control group showing branching and anastomosing cardiac muscle fibers. Cardiac myocytes have acidophilic sarcoplasm (zigzag arrows) and central oval nuclei (thin arrows). Muscle fibers are surrounded by thin connective tissue containing flat dark nuclei of fibroblasts (arrow heads) and blood vessels (BV). (A): (H &E x 200), (B): (H &E x 400).

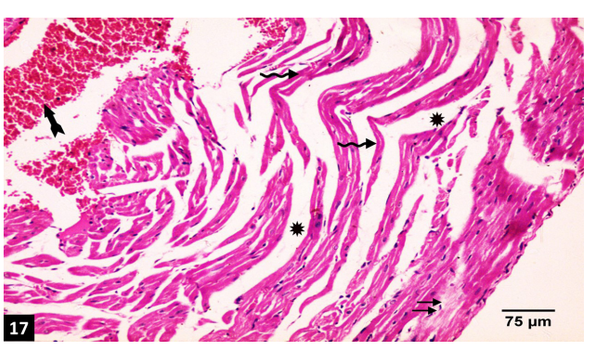

Fig.17: A photomicrograph of a section of cardiac muscle of group II (animals received low dose of Ag NPs) showing extravasated RBCs (bifid arrow) between cardiac muscle fibers. The muscle fibers appear wavy (zigzag arrow) with areas of decreased acidophilia (double thin arrows). Note the wide spaces between the muscle fibers (Asterisks). (H &E x 200)

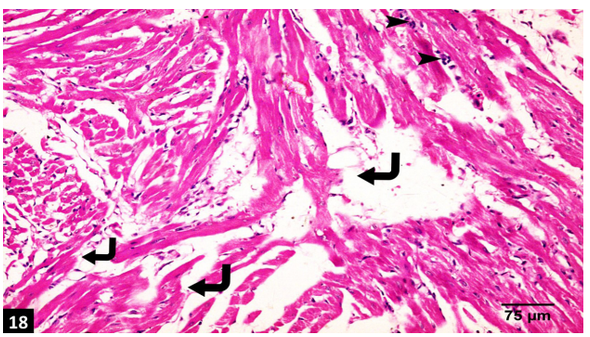

Fig.18: A photomicrograph of a section of cardiac muscle of group II (animals received low dose of Ag NPs) showing inflammatory cellular infiltration (arrow head) between the cardiac muscle fibers. Disorganization of the muscle fibers with interruption of some of them (right angle arrows) was also noticed. (H &E x 200).

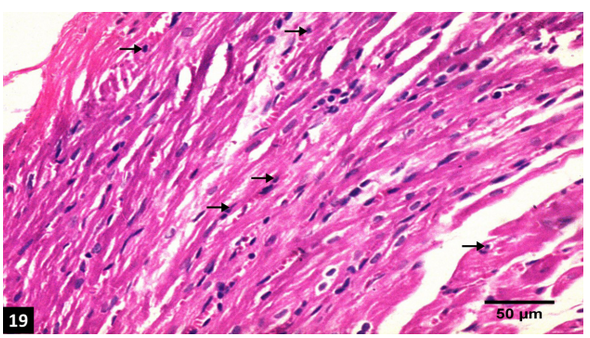

Fig.19: A photomicrograph of a section of cardiac muscle of group II (animals received low dose of Ag NPs) showing cardiac myocytes with pyknotic nuclei (arrows). (H &E x 400).

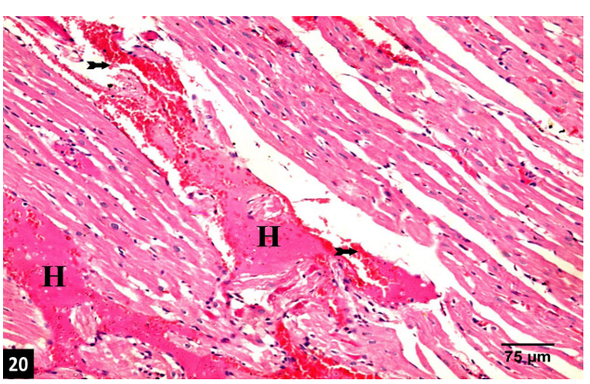

Fig.20: A photomicrograph of cardiac muscle of group III (animals received high dose of Ag NPs) showing extravasated RBCs (bifid arrows) between cardiac muscle fibers. Homogenous acidophilic material deposition (H) is also observed (H &E x 200).

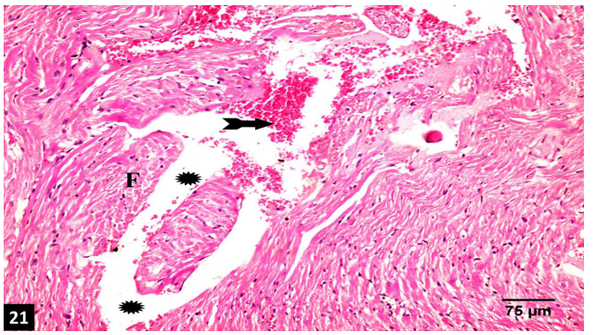

Fig.21: A photomicrograph of cardiac muscle of group III (animals received high dose of Ag NPs) showing extravasated RBCs (bifid arrows) between cardiac muscle fibers. Fragmented cardiac muscle fibers (F) and wide spaces between them (Asterisks) are observed. (H &E x 200).

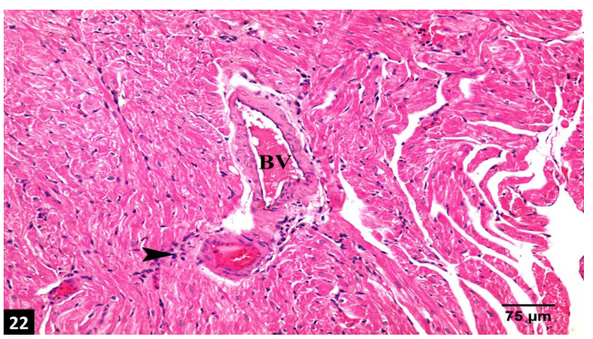

Fig.22: A photomicrograph of cardiac muscle of group III (animals received high dose of Ag NPs) showing dilated congested blood vessels (BV) and inflammatory cellular infiltration (arrow head). (H &E x 200)

.

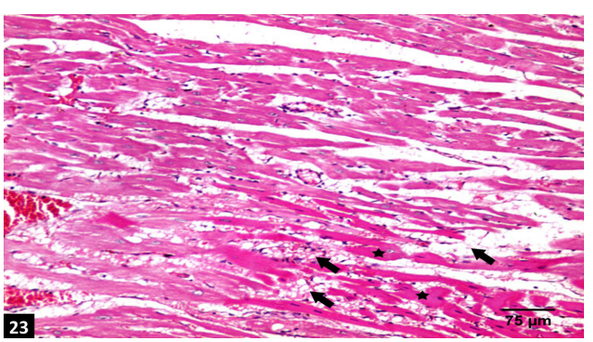

Fig.23: A photomicrograph of cardiac muscle of group III (animals received high dose of Ag NPs) showing vacuolated cardiac muscle fibers (thick arrows) with areas of hyper-acidophilia (stars). (H &E x 200).

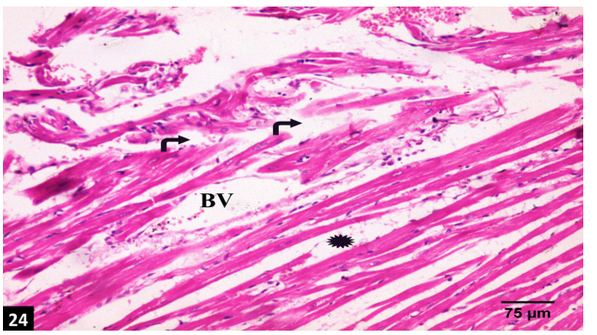

Fig.24: A photomicrograph of cardiac muscle of group III (animals received high dose of Ag NPs) showing dilated blood vessel (BV), disarrangement of the cardiac muscle fibers, interrupted fibers (right angle arrows) and wide spaces between them (Asterisks). (H &E x 200)

.

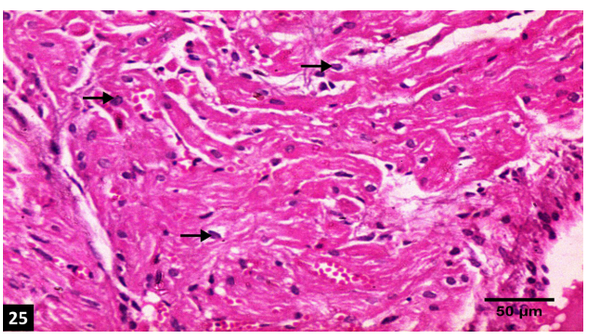

Fig.25: A photomicrograph of a section of cardiac muscle of group III (animals received high dose of Ag NPs) showing cardiac myocytes with pyknotic nuclei (arrows). (H &E x 400).

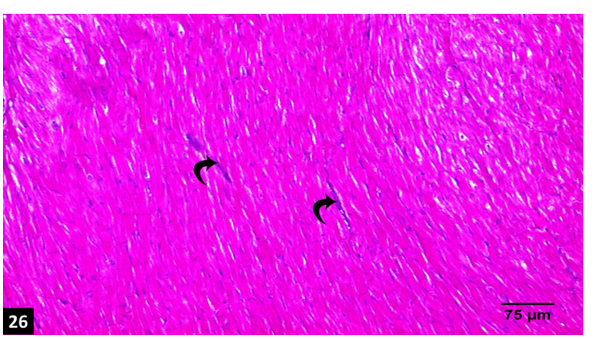

Fig.26: A photomicrograph of cardiac muscle from control group showing minimal amount of collagen fibers (curved arrows) between the cardiac muscle fibers. (Masson`s trichrome x 200).

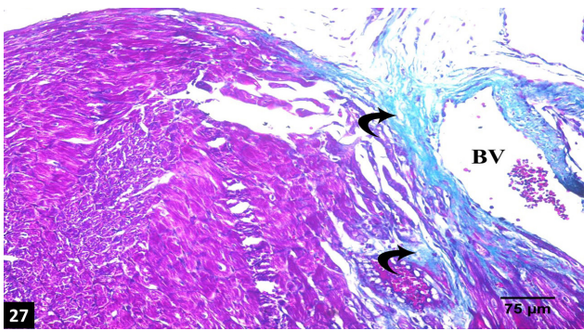

Fig.27: A photomicrograph of a section of cardiac muscle of group II (animals received low dose of Ag NPs) showing deposition of considerable amount of collagen fibers (curved arrows) in between the cardiac muscle fibers and around blood vessel (BV). (Masson`s trichrome x 200).

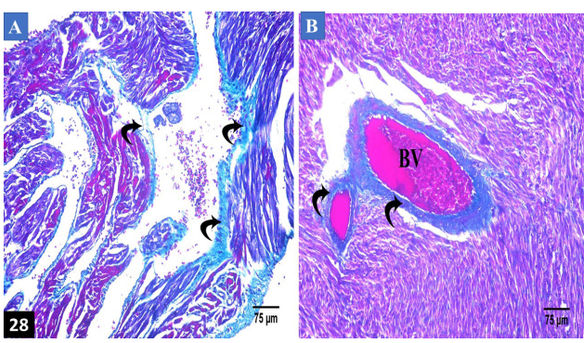

Fig.28: Photomicrographs of sections of cardiac muscle of group III (animals received high dose of Ag NPs) showing apparent increase in collagen fibers deposition (curved arrows) in between the cardiac muscle fibers and around dilated congested blood vessels (BV). (A &B) (Masson`s trichrome x 200).

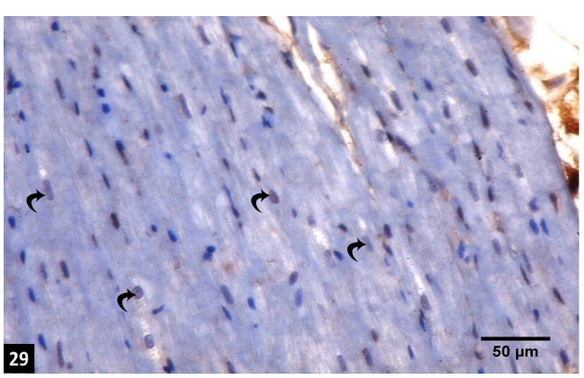

Fig.29: A photomicrograph of cardiac muscle from control group showing negative cleaved caspase3 reaction (curved arrows) in cardiac myocytes. (Cleaved caspase 3 x 400).

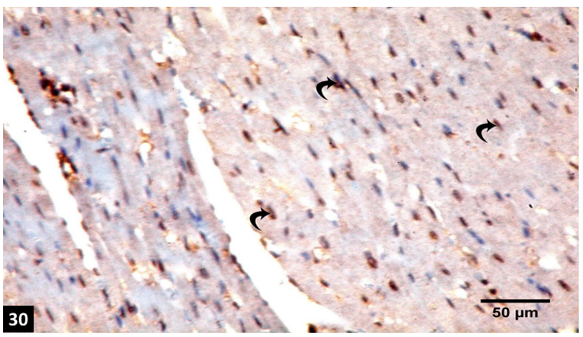

Fig.30: A photomicrograph of a section of cardiac muscle of group II (animals received low dose of Ag NPs) showing apparent moderate positive reaction for cleaved Caspase 3 (curved arrows) in some of cardiac myocytes. (Cleaved caspase 3 x 400).

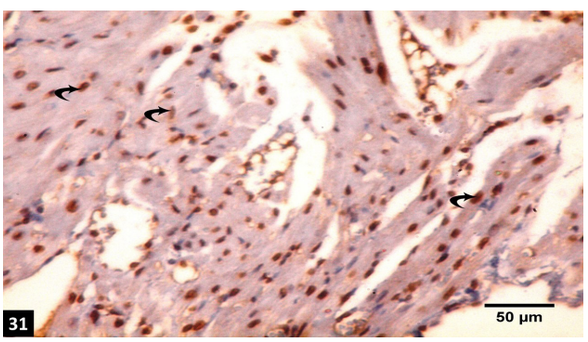

Fig.31: A photomicrograph of a section of cardiac muscle of group III (animals received high dose of Ag NPs) showing apparent strong positive reaction for cleaved caspase 3 (curved arrows) in many cardiac myocytes. (Cleaved caspase 3 x 400).

Table 1: Data are shown as Mean ± SD, (a) indicates a highly significant versus control, (b) indicates a significant versus control & (c) indicates a significant versus group II respectively.

	Group I	Group II	Group III
		Mean ± SD	
Mean area percentage of collagen fibers	1.79±0.42	3.95 ± 0.87[b]	5.11 ± 1.17[a]
Mean optical density of CD-68	1.21 ±0.11	1.40 ±0.05[b]	1.58 ±0.09[ac]

Table 2: Data are shown as Mean ± SD, (a) indicates a highly significant versus group I & (b) indicates a significant versus group I respectively.

	Group I	Group II	Group III
		Mean ± SD	
Mean area percentage of collagen fibers	1.24±0.58	2.71 ± 1.31	3.44 ± 1.01[b]
Mean optical density of cleaved caspase 3	1.06 ±0.03	1.22 ±0.06 [a]	1.29 ±0.06 [a]

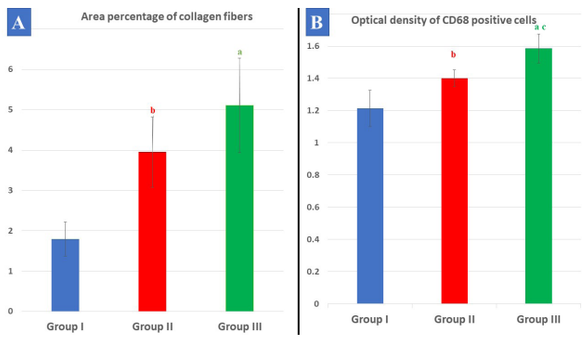

Histogram 1A,B: The area percentage of collagen fibers and the optical density of CD68 positive cells in lung sections in different studied groups

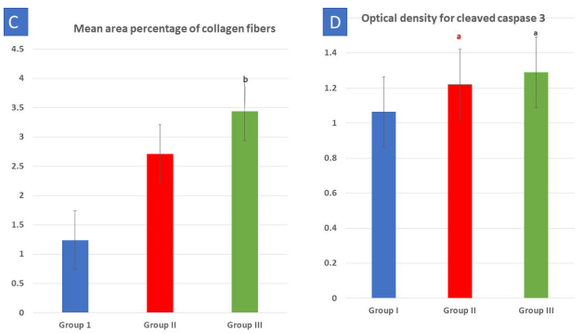

Histogram 2C,D: The mean area percentage of collagen fibers and the optical density for cleaved Caspase 3 in cardiac muscle sections of the studied groups

DISCUSSION

Ag NPs have gained popularity recently as a result of their widespread use in diagnostics, biomarkers, cell labelling, antimicrobial agents, drug administration, and cancer therapy[31]. Thus, too many people are exposed to Ag NPs through oral route, skin contact, inhalation, subcutaneous injection, and intravenous injection. Ag NPs are distributed, after their absorption, in various biological organs including the dermal, respiratory, digestive, urinary, nervous, immunological, and reproductive systems, producing toxic effects to these biological organs and systems[32].

Nanoparticles enter the respiratory system through inhaled particles making it an attractive target for nanoparticle toxicity. Nanoparticles also may indirectly affect lung function even if they don't deposit there. Heart problems like dysfunction, dysrhythmia, heart failure, and infarction can all be brought on by being exposed to NPs[33,34].

Several studies investigated the harmful effect of Ag NPs on heart and lung cell lines in vitro[35,36]. Other researchers investigated the cytotoxic impact of various Ag NPs sizes[37]. While other authors studied the effect of different sizes of Ag NPs on different vital organs as liver, kidney, and testis[18,38,39]. So, this research was created to examine in vivo effects of 2 different doses of Ag NPs on lung and cardiac muscle histology of adult female albino rats.

Several mechanisms explained cytotoxicity induced by Ag NPs including oxidative stress, lipid peroxidation, silver ion dissolution, apoptosis, necrosis, and autophagy. Oxidative stress is caused when there's a discrepancy between how much ROS is produced and how fast a biological system can get rid of reactive intermediates or repair the damage they cause. ROS that are produced nearby or inside the cell may be the direct cause, or they may also have an indirect effect on mitochondrial respiration or deplete antioxidant species within the cell[34]. Vuković *et al*[12] noted that ROS production and mitochondrial membrane potential depletion cause oxidative DNA and structural protein damage, cytotoxicity, programmed cell death, genotoxicity, immune system activation/suppression, and lipid peroxidation of biological membranes. Another explanation of nanoparticle cytotoxicity was reported by some authors[40, 41] who found that nanoparticle exposure caused lipid peroxidation, which in turn altered membrane physical properties, led to covalent modification of proteins, and could harm the entire cell (mitochondria, nucleus, and endoplasmic reticulum). This was in a line with previous studies that showed Ag NPs caused ultrastructural changes in hepatocyte nuclei, mitochondria, and RER[38].

Additionally, one of the mechanisms that could also explain Ag NPs induced cytotoxicity is the "Trojan-horse" mechanism. In this case Ag NPs enter the cells and inside the acidic medium of lysosomes, they are chemically transformed into elemental silver, Ag+, Ag-O- and Ag-S- species. The released silver ions (Ag+) would bind intracellular sulfhydryl group (−SH)-containing molecules such as glutathione S-transferase (GST), myosin and peroxiredoxin. Depletion of GST activity (an important detoxification enzyme), by Ag NPs leads to cytotoxicity [32, 41]. Talarska et al.[42] explained that the accumulation of ROS, a byproduct of the electron transport chain, was what ultimately hindered mitochondrial function after Ag+ ions were released. This would damage mitochondria, impair their function, depolarize their membranes and affect their DNA as well as peroxide fats and proteins, causing apoptosis.

The present work revealed dose dependant structural changes in the lung and cardiac muscle tissues of rats treated with Ag NPs. In the lung, there were alveolar architecture disturbance with collapse of some alveoli and emphysematous dilation of others, thickening of the interalveolar septa, congested blood vessels, hemorrhage, and inflammatory cellular infiltration between alveoli and bronchioles. Some bronchiolar epithelial cells were vacuolated, while others were desquamated. Group III had worse changes than group II. Similar results were obtained by other authors[26,43,44]. Also, similar results were detected on studying the effect of variable sizes of Ag NPs on testicular tissue. These results included desquamation

of spermatocytes and cytoplasmic vacuolation[18].

The histopathological changes detected in lung sections of rats treated with Ag NPs could be clarified by Xiao *et al.*[45] who declared that damage of alveolar epithelial cells by nanoparticles, generated a large amount of cytokines. This allowed fibroblasts to multiply and differentiate into myofibroblasts, which generated collagen and other components of the extracellular matrix (ECM). Massive ECM deposition caused the alveolar septum to thicken, which ultimately resulted in loss of the lung tissue's normal structure and function. Gosselink *et al*,[46] demonstrated that whereas some tiny airways exhibited a thickened profile, others exhibited a comparable damage to the parenchyma.

Type II pneumocyte degeneration, which affects surfactant secretion and causes an increase in surface tension, may be a possible explanation for alveolar collapse. This was described in explanation of the pathogenesis of chronic obstructive pulmonary disease[47]. On the other hand, emphysematous dilatation might be linked to an abnormal lung inflammatory response to foreign substances, such as the nanoparticles used in this study. This resulted in the elastolysis or destruction of elastic fibers in alveolar septa by metalloproteinases. One of the characteristics of emphysema is elastolysis[48].

The bronchiolar epithelial cells' vacuolation and desquamated cells may be caused by cellular necrosis, which reduces the function of the transport membrane, allowing sodium and water to enter the cell, causing the cell and its organelles to swell. The same finding was observed by[29]. Additionally, Elbakary *et al*,[49] found these vacuoles following gold nanoparticle exposure and linked them to membrane dysfunction and the increased influx of sodium and water. Finally, this caused organelles to swell.

In Masson's trichrome stained sections, collagen fiber deposition was seen around dilated blood vessels, around the bronchioles, and in the interstitium of lung. In group III, collagen fiber percentage area showed a highly significant elevation compared to control group., that was declared by Qian *et al*.[50] and Zhu *et al*.,[51]. They showed a connection between exposure to NPs and lung fibrosis. Inflammation causes pulmonary fibrosis, which is characterized by high levels of proinflammatory cytokines, C-reactive protein, tissue plasminogen activator, and nuclear transcription factor. -Kappa-B. These factors directly upregulate lung profibrotic transforming growth factor-beta 1 genes, which increases hydroxyproline content, fibronectin production, and type I collagen by activated fibroblasts, promotes epithelial mesenchymal transformations into myofibroblasts, and inhibits ECM-degrading proteases, causing severe pulmonary fibrosis.

Obvious CD-68 immunoreaction detected in the lung sections from rats of group II and III and was confirmed statistically could be explained as a defense mechanism of the macrophages that react to external insults as nanoparticles in the lung[52]. Interstitial macrophages, on the other hand, are a different class of macrophages that serve as a second line of defense against harmful substances that come into contact with the lungs because they play crucial immune roles that include preserving lung homeostasis and mediating allergic reactions in the airways[53]. All lung macrophages produce cytokines and contribute to adaptive immunity[54]. This result matched with[29,55]. Also, Al-Doaiss *et al*[39] detected hyperplasia of liver macrophages, Kupffer cells, mainly in the liver of mice exposed to 20 nm Ag NPs while investigating the effect of different sizes of Ag NPs on the liver.

Regarding H&E-stained cardiac muscle specimens from rats treated with Ag NPs, dilated blood vessels, extravasated RBCs, inflammatory cellular infiltration, and vacuolation were present. Cardiac muscle fibers exhibited foci of muscle hyalinosis, fragmentation, interruption, areas of low acidophilia and hyper-acidophilic areas. Wide spaces between the fibers were also observed. As regards cardiac myocytes, pyknotic nuclei were observed. The changes were also noticed in group III than group II. Similar results were reported by other authors[56, 57&58].

Disruption of cardiac muscle fibers including fragmentation, interruption, low acidophilia and wide spaces between them that was detected in this research could be explained by excessive intracellular Ca^2 levels induced by Ag NPs cytotoxicity. High Ca^{2+} levels caused sustained myofibrillar contraction, ATP depletion, and ROS-induced lipid peroxidation. Self-sustaining myolytic cascade caused massive cardiac muscle necrosis and muscle disintegration[59].

In the current study, foci of muscle hyalinosis (homogeneous acidophilic sarcoplasmic regions) were noted. Okasha and Ragab,[60] demonstrated that decreased myofibrillar protein synthesis and increased protein degradation might be the causes of the degeneration of cardiac myocytes. Reactive free radical buildup might promote cytosolic lysosomal enzyme release, where the oxidation of these myofibrils' protein backbones would result in their fragmentation.

Increased eosin binding to the denatured cytoplasmic proteins may be a contributing factor to the hyper-acidophilia seen in some cardiac myocytes of group III[58].

Vacuolation of cardiac muscle fibers that was observed in group III might be fatty degeneration in dead cardiomyocytes. This finding was also noted by[61,62] who claimed that fibrocytes became adipocytes at scar tissue edges with preserved blood flow.

In the present work, pyknotic nuclei of cardiac myocytes could be attributed to apoptosis induced by Ag NPs. This was confirmed by obvious cleaved caspase 3 immunoreaction detected in cardiac muscle sections from rats of group II and III and statistically confirmed by a highly significant increase in cleaved caspase 3 mean optical density in group II and III when compared to group I. Ferdous & Nemmar,[17] examined mice's cardiovascular responses to Ag NPs inhalation at various

coatings, concentrations, and exposure times. Their research demonstrated that inhaling Ag NPs caused lung inflammation, heart oxidative DNA damage and apoptosis, altered coagulation markers, and thrombosis. This finding confirmed by Yousef *et al*,[63] who showed cardiac myocyte apoptosis, inflammation, and fibrosis on Ag NPs exposure. Similar finding was reported by some authors on studying the effect of Ag NPs on neurons[64].

Collagen fibers were seen to accumulate around dilated congested blood vessels and in-between cardiac muscle fibers. This result was clear in group III, and it was statistically supported by the significant rise in the mean percentage area of collagen fibers in that group relative to group I. The same observation was documented by Zoheir *et al*.[58] who asserted that NPs toxicity was also mediated by ROS-mediated activation of fibrogenesis. Proliferation, migration, and trans-differentiation of fibroblasts into myofibroblasts, which produced significant amounts of interstitial collagen, were all induced by myocardial injury.

Cellular infiltrations and extravasation detected in this study in both lung and cardiac muscle specimens, were also demonstrated by Alarifi *et al*.[65] and Setyawati *et al*.[66] who claimed that endothelial integrity and permeability of cells were both affected by how NPs interact with vascular endothelium cadherin, leading to its disruption. This would also attract peripheral immune cells, causing inflammation and hemorrhage. Elsabahy & Wooley[67] and Mukherjee *et al*.[68] demonstrated that immune cells perceived silver nanomaterials as foreign substances; consequently, after internalization by cells, nanoparticles could cause cytokines and chemokines production. Blood levels of macrophages and inflammatory cells rose after the release of these chemical mediators. This triggered a series of subsequent events that included numerous cytokines expression, including TNF-α, different types of interleukins, and an inflammatory response, which removed the nanoparticles through phagocytosis by the inflammatory cells.

Additionally, vascular changes as dilatation and congestion of blood vessels that were observed could be explained because of inflammation to endothelial cells. This demonstration was suggested by Trickler *et al*.[69] who showed that Ag NPs induced dose-, time-, and size-dependent inflammation in human blood-brain barrier microvessel endothelial cells. Other Ag NP studies on the spleen reached similar conclusions[70].

CONCLUSION AND RECOMMENDATIONS

Lung and cardiac muscle undergo dose-dependent structural changes when exposed to Ag NPs. So, caution should be taken on exposure to Ag NPs especially in females. Further studies are needed to demonstrate if there is recovery of the effect of nanoparticles after their cessation.

CONFLICT OF INTERESTS

There are no conflicts of interest

REFERENCES

1. Ema, M., Okuda, H., Gamo, M. & Honda, K.: A review of reproductive and developmental toxicity of silver nanoparticles in laboratory animals. Reproductive Toxicology. (2017); 67,149-164.doi: 10.1016/j. reprotox.2017.01.005.
2. Khan, A. U., Malik, N., Khan, M., Cho, M. H., & Khan, M. M.: Fungi-assisted silver nanoparticle synthesis and their applications. Bioprocess and biosystems engineering. (2018); 41(1), 1-20. doi: 10.1007/s00449-017-1846-3.
3. Rafique, M., Sadaf, I., Rafique, M.S. & Tahir, M.B.: A review on green synthesis of silver nanoparticles and their applications. Artif Cells Nanomed Biotechnol. (2017); 7 (7),1–20. doi:10.1080/21691401.2016. 1241792.
4. Khan, I., Saeed, K., & Khan, I.: Nanoparticles: Properties, applications and toxicities. Arabian journal of chemistry. (2019); 12(7), 908-931. https://doi. org/10.1016/j.arabjc.2017.05.011.
5. Gurunathan, S., Park, J. H., Han, J. W., & Kim, J. H.: Comparative assessment of the apoptotic potential of silver nanoparticles synthesized by Bacillus tequilensis and Calocybe indica in MDA-MB-231 human breast cancer cells: targeting p53 for anticancer therapy. International journal of nanomedicine. (2015);10, 4203-4205. doi: 10.2147/IJN. S83953.
6. Gitipour, A., Thiel, S. W., Scheckel, K. G., & Tolaymat, T.: Anaerobic toxicity of cationic silver nanoparticles. Science of the total Environment. (2016); 557, 363-368. doi: 10.1016/j.scitotenv.2016.02.190
7. Gatto, F. & Bardi, G.: Metallic nanoparticles: General research approaches to immunological characterization. Nanomaterials. (2018); 8(10), 753. doi: 10.3390/nano8100753.
8. Almansour, M., Jarrar, Q., Battah, A., Obeidat, F., Khairat Battah, K., Jarrar, B.: Renal histopathological alterations induced by nanosilver toxicity: the size effect. (2016). IET Micro and Nano Letters, 11(12):862-865.
9. Almansour, M., Jarrar, Q., Battah, A., Obeidat, F., Khairat Battah, K., Jarrar, B. Hepatic histopathological and histochemical alterations induced by the toxicity of different sizes of silver nanoparticles. (2015). Ciência e Técnica Vitivinícola, 30 (8): 100-123.
10. Castro-Aceituno, V., Ahn, S., Simu, S. Y., Singh, P., Mathiyalagan, R., Lee, H. A. & Yang, D. C.: Anticancer activity of silver nanoparticles from Panax ginseng fresh leaves in human cancer cells. Biomedicine & Pharmacotherapy. (2016); 84, 158-165. doi: 10.1016/j. biopha.2016.09. 016.
11. Malik, P. & Mukherjee, T. K.: Recent advances in gold and silver nanoparticle-based therapies for lung and breast cancers. International Journal of Pharmaceutics. (2018); 553(1-2), 483-509. doi: 10.1016/ j.ijpharm.2018.10.048.

12. Vuković, B., Milić, M., Dobrošević, B., Milić, M., Ilić, K., Pavičić, I., ... & Vrček, I. V.: Surface stabilization affects toxicity of silver nanoparticles in human peripheral blood mononuclear cells. Nanomaterials. (2020); 10 (7), 1390. https://doi.org/10.3390/nano10071390.

13. Pourzahedi, L., Vance, M. & Eckelman, M. J.: Life cycle assessment and release studies for 15 nanosilver-enabled consumer products: investigating hotspots and patterns of contribution. Environmental Science & Technology. (2017); 51(12), 7148-7158. doi: 10.1021/acs.est.6b05923.

14. De Matteis, V.: Exposure to inorganic nanoparticles: routes of entry, immune response, biodistribution and in vitro/in vivo toxicity evaluation. Toxics. (2017); 5(4), 29. doi: 10.3390/toxics5040029.

15. Boudreau, M. D., Imam, M. S., Paredes, A. M., Bryant, M. S., Cunningham, C. K., Felton, R. P., ... & Olson, G. R.: Differential effects of silver nanoparticles and silver ions on tissue accumulation, distribution, and toxicity in the Sprague Dawley rat following daily oral gavage administration for 13 weeks. Toxicological Sciences. (2016); 150(1), 131-160. doi: 10.1093/toxsci/kfv318.

16. Deshmukh, S. P., Patil, S. M., Mullani, S. B., & Delekar, S. D.: Silver nanoparticles as an effective disinfectant: A review. Materials Science and Engineering: C. (2019); 97, 954-965. doi: 10.1016/j.msec.2018.12.102.

17. Ferdous, Z.& Nemmar, A.: Health impact of silver nanoparticles: a review of the biodistribution and toxicity following various routes of exposure. International Journal of Molecular Sciences. (2020); 21(7), 2375. https://doi.org/10.3390/ijms21072375.

18. Almansour M, Jarrar Q, Battah A, Jarrar B.:Histomorphometric Alterations Induced in the Testicular Tissues by Variable Sizes of Silver Nanoparticles. (2017). Journal of Reproductive Medicine, 62(3):317-323.

19. Konnova, S. A., Danilushkina, A. A., Fakhrullina, G. I., Akhatova, F. S., Badrutdinov, A. R. & Fakhrullin, R. F.: Silver nanoparticle-coated "cyborg" microorganisms: rapid assembly of polymerstabilised nanoparticles on microbial cells. RSC Adv., (2015); 5(18), 13530-13537. Retrieved from http://pubs.rsc.org/en/content/articlehtml/2015/ra/c4ra158 57a.

20. Nosrati H., Hamzepoor M., Sohrabi M., Saidijam M., Mahmoudian Z.G. & Alizadeh Z.: The potential renal toxicity of silver nanoparticles after repeated oral exposure and its underlying mechanisms. BMC Nephrology. (2021); 22:228. https://doi.org/10.1186/s12882-021-02428-522.

21. Yousof, S.M., Erfan, H., Hosny, M.M., Shehata,S.A. & El-Sayed, K.: Subacute toxic effects of silver nanoparticles oral administration and withdrawal on the structure and function of adult Albino Rats' hepatic tissue. Saudi Journal of Biological Sciences. (2022); 29:3890-3898. https://doi.org/10.1016/j.sjbs.2022.02.054.

22. Ghasi S., Umana I., Ogbonna A., Nwokike M. & Ufelle S.: Cardioprotective effects of animal grade piperazine citrate on isoproterenol induced myocardial infarction in wistar rats: Biochemical and histopathological evaluation. African Journal of Pharmacy and Pharmacology. (2020); 14(8): 285-93. https://doi.org/10.5897/AJPP2020.5164.

23. Bancroft, J.D. and Layton, C.: The hematoxylins and eosin in Bancroft's Theory and Practice of Histological Techniques (editors: Suvarna, S.K., Layton, C., Bancroft, J.D)., 8th ed. Philadelphia, USA: Elsevier; chapter 10; 2019:126–138.

24. Bancroft, J. and Layton, C.: Connective and mesenchymal tissues with their stains in Bancroft's Theory and Practice of Histological Techniques (editors: Suvarna SK, Layton C and Bancroft JD). 7th ed. Philadelphia: Churchill Livingstone Elsevier; chapter 11; 2013: P:187-214.

25. Jackson, P. and Blythe, D.: Immunohistochemical techniques in Bancroft's Theory and Practice of Histological Techniques. (editors: Suvarna SK, Layton C, Bancroft JD). 7th ed. Philadelphia: Churchill Livingstone; chapter 18; 2013: 381–426.

26. Abd El-Galil & M.M. and Alkot, A.M.F.: Impact of crude aloe vera gel on silver nanoparticle-induced lung cytotoxicity in adult male albino rats: Functional, histological and immunohistochemical study., Al-Azhar Med. J. (Medicine).(2022);51(1),563-604. https://amj.journals.ekb.eg/ article_212647.html.

27. El-Marasy, S.A., El Awdan, S.A., Hassan,A., Heba M.I. & Abdallah, H.M.I., : Cardioprotective effect of thymol against adrenaline-induced myocardial injury in rats., Heliyon 6 (2020); e04431.https://doi.org/10.1016/j.heliyon.2020.e04431.

28. Saleh, S.A., Algharabawy, G.S. & Hablas, M.G.: Comparative Histological and Immunohistochemical Study on The Effect of Curcumin and Atorvastatin in Induced Atherosclerosis in Aorta and Cardiac Muscle of Male Rabbits., The Egyptian Journal of Hospital Medicine. 2019; 76 (2), 3500-3515. doi: 10.21608/EJHM.2019.38653.

29. Gawish, M.F., Shaban, S.F., Abdel Aal S.M. & Shalabi S.S.: Effect of Silver Nanoparticles Versus Titanium Dioxide Nanoparticles on the Lung of Adult Male Albino Rats: A histological and immunohistochemical study. Journal of medical histology. (2018);2, (2), 181-200. doi: 10.21608/jmh.2019.12054.1055.

30. Emsley, R. Dunn, G. & White, I.R.: Mediation and moderation of treatment effects in randomised controlled trials of complex interventions. Statistical methods in medical research. (2010); 19, (3):237-70. doi: 10.1177/0962280209105014.

31. Mousavi, S. M., Hashemi, S. A., Ghasemi, Y., Atapour, A., Amani, A. M., Savar Dashtaki, A., ... & Arjmand, O.: Green synthesis of silver nanoparticles toward bio and medical applications: review study. Artificial cells, nanomedicine, and biotechnology, (2018); 46(sup3), S855-S872. doi: 10.1080/21691401.2018.1517769.

32. Xu, L., Wang, Y. Y., Huang, J., Chen, C. Y., Wang, Z. X., & Xie, H.: Silver nanoparticles: Synthesis, medical applications and biosafety. Theranostics, (2020); 10 (20), 8996-9031. doi:10.7150/thno. 45413.

33. Schulz, H., Harder, V., Ibald-Mulli, A., Khandoga, A., Koenig, W., Krombach,F., Radykewicz, R., Stampfl, A., Thorand,B., & Peters, A.: Cardiovascular effects of fine and ultrafine particles. Journal of aerosol medicine: the official journal of the International Society for Aerosols in Medicine. 2005;18(1):1-22. DOI: 10.1089/jam.2005.18.1.

34. Lu, X., Zhu, T., Chen, C., & Liu, Y.: Right or left: the role of nanoparticles in pulmonary diseases. International journal of molecular sciences, (2014) ;15(10), 17577-17600. https://doi.org/10.3390/ijms1510 17577.

35. Khan, A. A., Alanazi, A. M., Alsaif, N., Al-Anazi, M., Sayed, A. Y., & Bhat, M. A.: Potential cytotoxicity of silver nanoparticles: Stimulation of autophagy and mitochondrial dysfunction in cardiac cells. Saudi Journal of Biological Sciences, (2021); 28(5), 2762-2771. doi: 10.1016/j.sjbs.2021.03.021.

36. Li, L., Bi, Z., Hu, Y., Sun, L., Song, Y., Chen, S., ... & Wei, X.: Silver nanoparticles and silver ions cause inflammatory response through induction of cell necrosis and the release of mitochondria in vivo and in vitro. Cell Biology and Toxicology, (2021); 37(2), 177-191. doi: 10.1007/s10565-020-09526-4.

37. Gliga, A.R., Skoglund, S., Odnevall Wallinder, I. Fadeel, B.& Karlsson, H.L.:Size-dependent cytotoxicity of silver nanoparticles in human lung cells: The role of cellular uptake, agglomeration and Ag release. Part. Fibre Toxicol. (2014); 11, 11. http://www.particlean dfibretoxicology.com/content/11/1/11.

38. Almansour, M., Sajti, L., Melhim, W., & Jarrar, B. M.: Ultrastructural hepatocytic alterations induced by silver nanoparticle toxicity. (2016) Ultrastructural pathology, 40(2), 92-100.

39. Al-Doaiss, A. A., Jarrar, Q., Alshehri, M., & Jarrar, B.: In vivo study of silver nanomaterials' toxicity with respect to size. (2020). Toxicology and Industrial Health, 36(8), 540-557.

40. Gaschler, M.M. and Stockwell, B.R.: Lipid peroxidation in cell death. Biochem Biophys Res Commun. (2017) ;482(3):419–425. doi: 10.1016/j.bbrc.2016.10.086.

41. Rohde, M. M., Snyder, C. M., Sloop, J., Solst, S. R., Donati, G. L., Spitz, D. R., ... & Singh, R.: The mechanism of cell death induced by silver nanoparticles is distinct from silver cations. Particle and fibre toxicology, (2021); 18(37), 1-24. doi: 10.1186/s12989-021-00430-1.

42. Talarska, P., Boruczkowski, M., & Żurawski, J.: Current knowledge of silver and gold nanoparticles in laboratory research—Application, toxicity, cellular uptake. Nanomaterials, (2021); 11(9), 2454. https://doi.org/10.3390/nano11092454.

43. Ahmed, A. A., Hasan, R. A. & ElSayed, S. B.: Toxicological and Histological Effects of Silver Nanoparticles on The Lung of Adult Male Albino Rat and Protective Role of Green Tea Extract. The Egyptian Journal of Forensic Sciences and Applied Toxicology, (2016); 16(2), 55-78. doi: 10.21608/EJFSAT.2016.41010.

44. Moradi-Sardareh, H., Basir, H. R. G., Hassan, Z. M., Davoudi, M., Amidi, F. & Paknejad, M.: Toxicity of silver nanoparticles on different tissues of Balb/C mice. Life sciences, (2018); 211, 81-90. doi: 10.1016/j.lfs.2018.09.001.

45. Xiao, H., Huang, X., Wang, S., Liu, Z., Dong, R., Song, D. & Dai, H.: Metformin ameliorates bleomycin-induced pulmonary fibrosis in mice by suppressing IGF-1. American Journal of Translational Research, (2020); 12(3), 940-949. ISSN:1943-8141/AJTR0100078.

46. Gosselink, J. V., Hayashi, S., Elliott, W. M., Xing, L., Chan, B., Yang, L., ... & Hogg, J. C.: Differential expression of tissue repair genes in the pathogenesis of chronic obstructive pulmonary disease. American journal of respiratory and critical care medicine, (2010); 181(12), 1329-1335. doi: 10.1164/rccm.200812-1902OC.

47. Zhao, C.Z., Fang, X.C., Wang, D., Tang, F.D.& Wang, X.D.: Involvement of type II pneumocytes in the pathogenesis of chronic obstructive pulmonary disease. Respiratory Medicine. (2010); 104(10): 1391-1395. doi: 10.1016/j.rmed.2010.06.018.

48. Rodrigues, S. D. O., Cunha, C. M. C. D., Soares, G. M. V., Silva, P. L., Silva, A. R., & Gonçalves-de-Albuquerque, C. F.: Mechanisms, pathophysiology and currently proposed treatments of chronic obstructive pulmonary disease. Pharmaceuticals, (2021); 14(10), 979. doi: 10.3390/ph14100979.

49. Elbakary, R.H., Okasha, E.F., Hassan Ragab A.M. & Ragab, M.H.: Histological effects of gold nanoparticles on the lung tissue of adult male albino rats. J Microsc Ultrastruct, (2018) ;6 (2):116-122. doi: 10.4103/JMAU.JMAU_25_18.

50. Qian, F., He, M., Duan, W., Mao, L., Li, Q., Yu, Z., Zhou, Z.& Zhang, Y.: Cross regulation between hypoxiainducible transcription factor1α (HIF1α) and transforming growth factor (TGF)ß1 mediates nickel oxide nanoparticles (NiONPs)induced pulmonary fibrosis. Am J Transl Res, (2015); 7(11): 2364-2378. www.ajtr.org /ISSN:1943-8141/AJTR0014859.

51. Zhu, X., Cao, W., Chang, B., Zhang, L., Qiao, P., Li, X., Si, L., Niu, Y.& Song, Y.: Polyacrylate/nanosilica causes pleural and pericardial effusion, and pulmonary fibrosis and granuloma in rats similar to those observed in exposed workers. International Journal of Nanomedicine., (2016);11: 1593–1605. doi:10.2147/ IJN.S102020.

52. Tanabe, N., McDonough, J. E., Vasilescu, D. M., Ikezoe, K., Verleden, S. E., Xu, F., ... & Hogg, J. C.: Pathology of idiopathic pulmonary fibrosis assessed by a combination of microcomputed tomography, histology, and immunohistochemistry. The American Journal of Pathology, (2020); 190 (12), 2427-2435. doi: 10.1016/j.ajpath.2020.09.001.

53. Schyns, J.; Bureau, F.; Marichal, T.: Lung Interstitial Macrophages: Past, Present, and Future. J. Immunol. Res. (2018); 2018, 1–10. doi: 10.1155/2018/5160794.

54. Hu, G.& Christman, J. W.: Alveolar macrophages in lung inflammation and resolution. Frontiers in immunology, (2019); 10, 2275. https://doi. org/10.3389/fimmu.2019.02275.

55. Song, K. S., Sung, J. H., Ji, J. H., Lee, J. H., Lee, J. S., Ryu, H. R., ... & Yu, I. J.: Recovery from silver-nanoparticle-exposure-induced lung inflammation and lung function changes in Sprague Dawley rats. Nanotoxicology, (2013); 7(2), 169-249. doi: 10.3109/17435390. 2011.648223.

56. Rathore, M., Mohanty, I. R., Maheswari, U., Dayal, N., Suman, R., & Joshi, D. S.: Comparative in vivo assessment of the subacute toxicity of gold and silver nanoparticles. Journal of nanoparticle research, (2014); 16(4), 2338. doi:10.1007/s11051-014-2338-x.

57. Adeyemi, O. S. & Faniyan, T. O.: Antioxidant status of rats administered silver nanoparticles orally. Journal of Taibah University Medical Sciences, (2014); 9(3), 182-186. https://doi.org/10.1016/j.jtumed.

58. Zoheir, M., Medwar, A., Solaiman, A., & Elbanawany, N.: Histological Study of the Effect of Zinc Oxide Nanoparticles on the Cardiomyocytes of Adult Male Albino Rats with Reference to the Role of Mitochondria. Egyptian Journal of Histology, (2019); 42(3), 567-582. doi: 10.21608/EJH.2019.7112.1065

59. Manuel, A. R. L., Martinez-Cuevas, P. P., Rosas-Hernandez, H., Oros-Ovalle, C., Bravo-Sanchez, M., Martinez-Castañon, G. A., & Gonzalez, C.: Evaluation of vascular tone and cardiac contractility in response to silver nanoparticles, using Langendorff rat heart preparation. Nanomedicine: Nanotechnology, Biology and Medicine, (2017). 13(4), 1507-1518.https://doi.org/10.1016/j.nano.2017.01.017.

60. Okasha, E.F. and Ragab, A.M.H.: Histological, Immunohistochemical and Ultrastructural Study on the Effect of Gold Nanoparticles on the Left Ventricular Cardiac Myocytes of Adult Male Albino Rat, Middle-East Journal of Scientific Research, (2015). 23 (12): 2968-2982, doi: 10.5829/idosi.mejsr.2015.23.12.10234.

61. Khater, N., Selim, S., Abd El-Baset, S.& Abd El Hameed, S.: Therapeutic effect of mesenchymal stem cells on experimentally induced hypertensive cardiomyopathy in adult albino rats. Ultrastruct Pathol. (2017) ;41(1):36-50. https://doi.org/10.1080/01913123.2016.1260080.

62. Kashef, S.M. and. M. Elswaidy, N.R.: The possible role of Allicin in ameliorating Azithromycin induced cardiotoxicity in adult male albino rat: A histological and Immunohistochemical study, Egyptian Journal of Histology. (2021); 45, (3): 863-874. doi: 10.21608/ejh.2021.72878.1465.

63. Yousef, M. I., Abuzreda, A. A., & Kamel, M. A. N.: Cardiotoxicity and lung toxicity in male rats induced by long term exposure to iron oxide and silver nanoparticles. (2019); Experimental and therapeutic medicine, 18(6), 4329-4339. https://doi.org/10.3892/etm.2019.8108.

64. Ma, W., Jing, L., Valladares, A., . Mehta, S.L., Wang, Z., Andy, P., Li P.A. & Bang, J.J: Silver Nanoparticle Exposure Induced Mitochondrial Stress, Caspase-3 Activation and Cell Death: Amelioration by Sodium Selenite. Int J Biol Sci. (2015) ;11(8):860–867. doi: 10.7150/ijbs.12059.

65. Alarifi, S., Ali, D., Al-Doaiss, A.A., Ali, B.A., Ahmed, M. &Al-Khedhairy, A.A.: Histologic and apoptotic changes induced by titanium dioxide nanoparticles in the livers of rats. International Journal of Nanomedicine, (2013); 8: 3937-3943. doi: 10.2147/IJN.S47174.

66. Setyawati, M.I., Tay, C.Y., Chia, S.L., Goh, S.L., Fang, W., Neo. M.J. & Xie, J.P.: Titanium dioxide nanomaterials cause endothelial cell leakiness by disrupting the homophilic interaction of VE cadherin. Nature Communications, (2013); 4:1673: 1-12. doi: 10.1038/ncomms2655.

67. Elsabahy, M. &Wooley, K. L.: Cytokines as biomarkers of nanoparticle immunotoxicity. Chemical Society Reviews, (2013);42(12), 5552-5576.

68. Mukherjee, D., Royce, S. G., Sarkar, S., Thorley, A., Schwander, S., Ryan, M. P., ... & Georgopoulos, P. G.: Modeling in vitro cellular responses to silver nanoparticles. Journal of Toxicology, (2014); 2014:852890. doi: 10.1155/2014/852890.

69. Trickler, W. J., Lantz, S. M., Murdock, R. C., Schrand, A. M., Robinson, B. L., Newport, G. D., ... & Ali, S. F.: Silver nanoparticle induced blood-brain barrier inflammation and increased permeability in primary rat brain microvessel endothelial cells. Toxicological Sciences, (2010); 118(1), 160-170. doi: 10.1093/toxsci/kfq244.

70. Mazen, N. F., Saleh, E. Z., Mahmoud, A. A., & Shaalan, A. A.: Histological and immunohistochemical study on the potential toxicity of sliver nanoparticles on the structure of the spleen in adult male albino rats. Egyptian Journal of Histology, (2017); 40(3), 374-387. doi: 10.21608/EJH.2017.4662.

الملخص العربى

تأثير الجرعات المختلفة من جسيمات الفضة النانوية على الرئة و عضلة القلب لأنثى الجرذ الأبيض البالغ (دراسة نسيجية وهستوكيميائية مناعية)

سوزان السيد أبو النصر[١]، آية محمد حسن رجب[٢]، محمد حسن رجب[٣]، شيماء محمد زاهر[٤]

[١]قسم الهستولوجيا وبيولوجيا الخلية، [٣]قسم التشريح، كلية الطب، جامعة طنطا، مصر.

[٢]قسم الصحة الإنجابية وتنظيم الأسرة، المركز القومي للبحوث، الجيزة، مصر.

[٤]قسم الهستولوجيا وبيولوجيا الخلية، كلية الطب، جامعة حلوان، مصر.

المقدمة: هناك العديد من التطبيقات المحتملة لجسيمات الفضة النانوية ، والتي تشمل التشخيص وأنها المضادة للميكروبات وعلاج السرطان ،وهذا جعل منها موضوعًا شائعًا للدراسة في السنوات الأخيرة. وعلى الرغم من الأهمية والاستخدام على نطاق واسع لـجسميات الفضة النانوية إلا أنها قد تسبب تسمم بيئي وبشري.

الهدف من العمل: تقييم نتائج الجرعات المختلفة من جسيمات الفضة النانوية على الرئة وعضلة القلب لإناث الجرذان البيضاء البالغة باستخدام طرق الفحص النسيجية والهستوكيميائية المناعية.

المواد وطرق البحث: تم تقسيم ثلاثين أنثًى من الجرذان البيضاء البالغة عشوائياً إلى ثلاثة مجموعات : -المجموعة الأولى وهذه مثلت المجموعة الضابطة و المجموعة الثانية: تلقت (30 مجم / كجم) من جسيمات الفضة النانوية أما المجموعة الثالثة: تلقت (300 مجم / كجم) من جسيمات الفضة النانوية وكلا المجموعتين الثانية والثالثة تناولوا جسيمات الفضة عن طريق الفم مرة واحدة يوميًا لمدة أسبوعين وتمت معالجة عينات من نسيج الرئة و عضلة القلب من أجل تقنيات نسيجية وهستوكيميائية مناعية كما تم إجراء دراسات قياسية وإحصائية أيضاً.

النتائج: أظهرت عينات الرئة للحيوانات المعالجة بجسميات الفضة النانوية انكماشًا فى بعض الحويصلات الهوائية وانتفاخ لحويصلات أخرى وزيادة فى سمك الحاجز بين الحويصلات, كما لوحظ ترسب ألياف الكولاجين ،احتقان فى الأوعية الدموية مع وجود مناطق للنزيف كما تم رؤية الخلايا الالتهابية و لقد أظهرت النتائج المناعية الكيميائية زيادة في التفاعل السيتوبلازمي لـلسى دى 68 .

وأظهرت العينات من عضلة القلب وجود كرات الدم الحمراء المتسربة مع احتقان فى الأوعية الدموية. كما لوحظ أيضاً تسلل للخلايا الالتهابية ووجود فجوات فى ألياف عضلة القلب كما أظهرت ألياف عضلة القلب انقطاعًا مع وجود مسافات واسعة بينها وترسب ألياف الكولاجين بينها كما كانت هناك زيادة كبيرة في الكثافة البصرية للكاسباس 3 المشقوق في خلايا عضلة القلب. ولقد شهدت المجموعة الثالثة كل هذه التغييرات بدرجة أكبر من المجموعة الثانية.

الخلاصة: تشير نتائج الدراسة الحالية إلى أن التعرض لجسيمات الفضة النانوية قد يسبب تغيرات نسيجية وهستوكيميائية مناعية قلبية ورئوية والتى قد تؤثر على وظيفة هذه الأعضاء الحيوية.